THE JOURNAL OF PHYSICAL CHEMISTRY C

Article

pubs.acs.org/JPCC

Directing the Structure of Two-Dimensional Silica and Silicates

Andrei Malashevich,[†,‡] Sohrab Ismail-Beigi,[†,‡] and Eric I. Altman*[,†,§]

[†]Center for Research on Interface Structures and Phenomena, [‡]Department of Applied Physics, and [§]Department of Chemical and Environmental Engineering, Yale University, New Haven, Connecticut 06520, United States

Supporting Information

ABSTRACT: Density functional theory was used to assess the viability of approaches to controlling the structure of a recently discovered two-dimensional form of SiO_2. In accord with prior work, a hexagonal bilayer of mirror image planes of corner-sharing SiO_4 tetrahedra in six-membered rings yielded only a slightly higher energy than α-quartz. Structures including four- through eight-membered rings were evaluated and in certain cases found to be as little as 17 meV/Si higher in energy than the hexagonal bilayer. When either biaxial or uniaxial tensile strain was applied, combinations of eight-, six-, and four-membered rings became favored due to the lower density of structures with larger rings. These findings, together with experiments that reveal expansion of silica bilayers to match the lattice of metal substrates, suggest that epitaxial strain may be used to control the bilayer structure. Replacement of Si with Ge and Al as prototypical tetravalent and trivalent dopants was also investigated. Substituting Ge for Si was energetically unfavorable and offered no obvious advantage for structural control over pure SiO_2 bilayers. In contrast, Al substitution was energetically favorable and only minimally distorted the bilayer. It was found that while the hexagonal bilayer remained favored, the extra-framework electron donors K and H that accompany each Al preferred to occupy larger rings when possible, thus forcing Al to reside in large rings as well. This suggests that the bilayer structure may be controlled through substitution of Si for trivalent dopants and selection of extra-framework electron donors that favor larger rings.

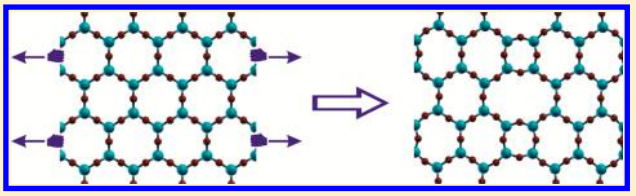

INTRODUCTION

The past decade has seen tremendous interest in atomically thin sheets that interact with each other and their surroundings solely through van der Waals interactions. The interest in such two-dimensional (2D) materials stems from unique physical properties that emerge as the dimensionality is reduced and the stability engendered by the lack of chemical interactions.[1−3] Recently, SiO_2 bilayers have been added to the family of 2D materials.[4−14] These bilayers are constructed from mirror image planes of corner-sharing SiO_4 tetrahedra and are considered to interact only through van der Waals forces.[4,10] Several features distinguish 2D SiO_2 from such widely studied 2D materials as graphene, BN, and dichalcogenides (e.g., MoS_2).[15] First, 2D SiO_2 is not derived by thinning a known bulk phase down to its atomic limit: there is no bulk analog of the single SiO_2 bilayer. Second, the flexibility of the SiO_4−SiO_4 linkages that gives rise to extremely rich silicate chemistry provides an avenue to tailor the structure and properties of the material.[16] This is already evidenced through its ability to form both crystalline and amorphous structures.[5,6,10−12] Finally, the flexibility coupled with the open structure provides opportunities to control how molecules pass through 2D layers,[17] thus potentially forming the basis for atomically thin molecular sieves. In this paper, we use first-principles density functional theory (DFT) to investigate how lattice strain and doping may be used to direct the structure of 2D SiO_2 away from the hexagonal structure favored by pure, unstrained 2D SiO_2 to structures containing larger openings or pores.

As illustrated in Figure 1a and Figure 1b, the crystalline form of 2D SiO_2 is constructed from a mirror image bilayer of six-membered rings of corner-sharing SiO_4 tetrahedra.[7,10] The amorphous form, Figure 1c, introduces four- through nine-membered rings, although the average ring size remains six.[6,7,18] In both cases, all the bonds are saturated explaining the van der Waals nature of the material.[10,19] Another consequence of the saturated bonds is that the exposed surfaces resemble the catalytically relevant internal surfaces of zeolites that are an intrinsic part of the bulk silicate structure and thus do not expose any dangling bonds.[8,20] This similarity has motivated the study of Al-doped 2D SiO_2 which has revealed similar acidities of the protonated forms of 2D aluminosilicates and Al-containing zeolite catalysts.[8,20−22] Evidence has also been reported for size-dependent passage of atoms through the centers of the rings to the underlying support.[23,24] Thus, 2D SiO_2 is both of fundamental interest as a surface science model of zeolite catalysts and of potential practical interest as an atomically thin size exclusion membrane.

For both fundamental and practical reasons, increased ring sizes are desired. On the practical side, comparing the 0.28 nm opening of the six-membered rings[25] (that define the crystalline phase and dominate the amorphous phase) with kinetic diameters suggests that only He (0.26 nm) and perhaps water (0.27 nm) and ammonia (0.26 nm) are small enough to

Received: July 14, 2016
Revised: October 28, 2016
Published: November 2, 2016

DOI: 10.1021/acs.jpcc.6b07008
J. Phys. Chem. C 2016, 120, 26770−26781

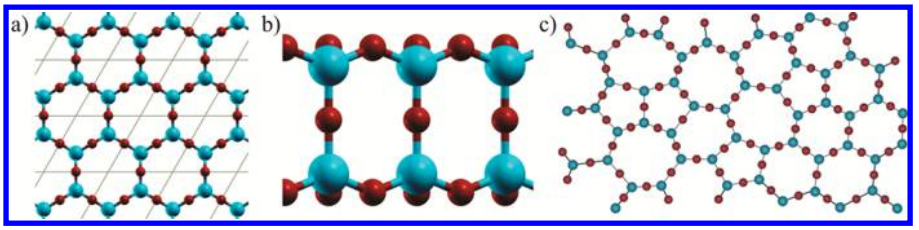

Figure 1. (a) Top and (b) side view of a ball and stick model of the crystalline hexagonal SiO_2 bilayer. (c) Model of the amorphous bilayer developed from a scanning tunneling microscopy image in ref 12. Cyan and red balls represent Si and O atoms, respectively. The thin solid lines in (a) indicate primitive 2D unit cells.

pass through the pores,[25−27] though there is experimental evidence that CO (0.38 nm), molecular hydrogen (0.29 nm), and O_2 (0.35 nm) can permeate the silica bilayers to adsorb on a metal substrate.[27−30] Depending on their shape, eight-membered rings can be large enough to allow molecules such as CO_2, CH_4, and C_2H_6 to move through the pores.[25,26] Extension to nine- and ten-membered rings would yield most of the size range found in zeolites which are well-known as molecular sieves and as size and shape selective catalysts.[26,31,32] Meanwhile, introducing the larger rings would also enable fundamental studies of the impact of bond angles and ring strain on the reactivity of zeolite frameworks.

Prior work indicates that strain and doping can influence the structure of 2D SiO_2.[33−35] The silica bilayers are typically formed by SiO_2 deposition and high temperature annealing on late transition metals, e.g., ruthenium, platinum, and palladium.[11,19,36] Despite the weak van der Waals interaction with the substrate, the silica layers stretch by 2.2% and 3.9% to match the atomic spacing of Ru(0001) and Pd(100), respectively.[4,11,19] On Pt(111) where 4.6% biaxial strain would be required for epitaxial growth of the crystalline form, only the amorphous structure is seen.[36] Meanwhile, elongated rings are seen at nearly ordered arrays of anti-phase domain boundaries (APBs) on Pd(100).[11] In contrast, the most commonly seen structure at APBs on the hexagonal Ru(0001) surface are eight-membered rings grouped with pairs of five-membered rings (hereafter referred to as $8{-}5^2$).[35] Curiously, when 2D SiO_2 on Ru(0001) is doped with Al, combinations of eight- and four-membered rings (8−4) replace the $8{-}5^2$ moiety as the predominant domain boundary structure.[35] In parallel, the ring size distribution of the amorphous phase broadens leading to an increase in the density of larger rings as the Al content increases.[35] There have been no systematic studies focused on understanding and exploiting these effects to manipulate the structure of the 2D material.

Motivated by these recent findings, we have employed DFT to investigate how strain and doping with tri- and tetravalent cations may be used to control the structure of 2D silicates. The results reveal that strain reduces the energy of structures containing larger rings, an effect that can be traced to the lower atomic areal density of the larger ring structures. In contrast, doping with trivalent Al does not intrinsically alter the energy differences between six-membered and larger rings. The electron donating species necessitated by Al substitution, however, prefer to sit in larger rings, suggesting that the choice of the donor may allow structure-control. Meanwhile, substituting Ge for Si yields highly distorted networks that are unlikely to form and otherwise offer no benefit over Si in terms of the sizes of the openings. Together the results indicate that lattice strain and co-doping with trivalent cations and large electron donors are the most viable routes to controlling the structure of 2D silica.

METHODS

The objective of this study was to screen for effects that may be exploited to direct the structure of 2D silica. As a result, a premium was placed on considering many different structures. To facilitate this goal, the work focused on free-standing bilayers in which the effect of the substrate was modeled by considering the epitaxial strain imparted by the substrate. Not including the substrate explicitly in the calculations is justified by prior work that reveal no chemical interactions between late transition metal substrates and SiO_2 bilayers which we confirmed in our calculations.[4,5,10] A recent study showed that van der Waals interactions can draw the SiO_2 layer close enough to Ru to induce some charge transfer from the SiO_2 bilayer to the metal;[37] the impact of this effect will be considered in continuing work.

The numerical simulations of bilayer silica were based on density functional theory (DFT) with the PBE generalized gradient approximation (GGA) for exchange and correlation.[38] The calculations of undoped silica were performed using the plane-wave pseudopotential approach as implemented in the Quantum ESPRESSO code package.[39] We employed Vanderbilt ultrasoft pseudopotentials.[40] The plane-wave basis energy and charge density cutoffs were set at 480 and 3800 eV, respectively. For all structures, the convergence with respect to *k*-point mesh density was verified. Due to the insulating nature of the systems, constant occupations were used for the Kohn−Sham electron states.

For doped silica, the calculations were performed using numeric atom-centered basis functions (NABF) using the FHI-AIMS code package.[41] For all calculations reported here, the "tight" basis set was employed. We verified on several selected systems that the calculations done with the different codes yield very similar ground state atomic structures and energy differences.

The silica bilayer structures were modeled using a slab geometry with periodic boundary conditions, and each slab was separated from its images by at least 15 Å of vacuum. The structural relaxations were performed until Cartesian components of forces on all atoms were less than 3 meV/Å in magnitude and in-plane stress tensor components were less than 0.1 kbar.

For calculations of strained silica, we assumed that the SiO_2 bilayers were grown on a Ru(0001) substrate. Therefore, the 2D lattice parameters of SiO_2 were chosen to be commensurate with the theoretically calculated lattice parameters of bulk Ru to mimic the strain effect from the substrate.

DOI: 10.1021/acs.jpcc.6b07008
J. Phys. Chem. C 2016, 120, 26770−26781

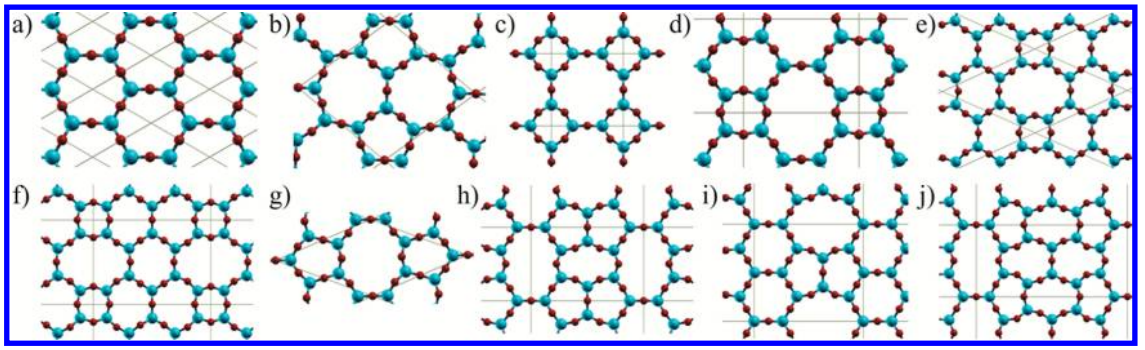

Figure 2. Models of silica bilayer structural motifs discussed in this paper: (a) hexagonal; (b) 7^2-5^2; (c) 8–4; (d) 8–6–4; (e) $8-6^2-4$; (f) $8-6^3-4$; (g) $8-5^2$; (h) $8-6-5^2$; (i) $8-6^2-5^2$; (j) $8-6^3-5^2$. The terminology $i^l-j^m-k^n$ refers to a unit cell with l i-membered rings, m j-membered rings, and n k-membered rings; the superscript is omitted when the ring size appears just once in the unit cell. Color scheme is as in Figure 1. Lines indicate primitive unit cells.

Table 1. Energy and Structural Properties of a Series of 2D SiO_2 Bilayer Structures[a]

motif	areal density, Si/Å^2	ΔE_f, meV/Si	ΔE_f, meV/unit cell	strained energy, meV/Si, 3.6% biaxial	strained energy, meV/Si, 3.6% uniaxial	strained energy, meV/Si, 2.2% biaxial	strained energy, meV/Si, 2.2% uniaxial
6	0.164	0.0	0	106.0	25.9	41.5	10.0
7^2-5^2	0.160	72.5	1161				
8–4	0.151	39.0	312				
8–6–4	0.158	32.3	388	71.5	37.5	50.9	44.6
$8-6^2-4$	0.160	26.1	417	75.1	28.1		
$8-6^3-4$	0.161	22.2	443	80.0	23.1	40.4	22.4
$8-5^2$	0.158	17.7	213				
$8-6-5^2$	0.164	33.1	529	1525.4	283.5		
$8-6^2-5^2$	0.161	39.3	786				
$8-6^3-5^2$	0.169	67.2	1612	991.3	235.8		

[a]Unstrained energy differences (ΔE_f) between hexagonal SiO_2 bilayers (labeled "6") and structural motifs incorporating different sized rings on per Si atom and per unit cell basis (all structures fully relaxed). The strained energies are referenced to the unstrained hexagonal bilayer. The 3.6% and 2.2% strains denote the strain imparted when the hexagonal bilayer is stretched to match twice the computed and experimental Ru a lattice constants, respectively. The terminology $i^l-j^m-k^n$ refers to a unit cell with l i-membered rings, m j-membered rings, and n k-membered rings; the superscript is omitted when the ring size appears just once in the unit cell.

RESULTS

Benchmarking Calculations. As described in the Methods section, calculations for bilayer silica were performed using a plane wave pseudopotential approach while doped silica was studied using numeric atom-centered basis functions (NABF);[41] in both cases the PBE generalized gradient approximation of the exchange–correlation potential was used.[38] We started our study of silica structures with a series of benchmarking calculations comparing the structural parameters and energetics of the α-quartz polymorph of bulk SiO_2 with crystalline hexagonal bilayers calculated with the plane-wave pseudopotential and NABF approaches, as well as a series of NABF calculations on reference materials needed to calculate doping energetics. The details of these calculations are provided in the Supporting Information. The salient points are the following: (1) the structures of the crystalline hexagonal bilayer calculated using the two methods agree with one another and experiment; (2) the energy of the crystalline hexagonal bilayer is only 40–50 meV/Si higher than α-quartz; (3) the energy of the prototypical zeolite chabazite also falls in this range; (4) the agreement between experiment and theory for a series of reference oxides used to calculate substitution energies is similarly good. One area where the calculations did not reproduce experimental observations was the relative energies of the octahedrally coordinated rutile and tetrahedrally coordinated α-quartz polymorphs of GeO_2. The calculations suggested that the two GeO_2 phases were nearly degenerate in energy (the α-quartz phase was 0.5 meV/Ge atom lower in energy) while experimentally the rutile phase is more stable with the α-quartz phase favored only at high temperatures.[42] As will be described below, the overestimate of the stability of tetrahedral GeO_2 does not impact the major conclusions of this paper which depend on the structures and relative energies of tetrahedrally coordinated phases.

Structural Moieties in 2D Silica. Starting from the hexagonal six-membered-ring structure, we introduced various ring sizes to investigate how the energy of the resulting structure depends on the ring motifs. Following expectations for planar tricoordinate networks, the average ring size in all motifs was fixed at six. In addition to six-membered rings, we considered four-, five-, seven-, and eight-membered rings which together with nine-membered rings comprise the experimentally observed amorphous structure and the common defects observed in the crystalline hexagonal phase.[5−7,10,12] The structural motifs considered in this work are shown in Figure 2. We label the motifs by specifying the sizes of all the rings in the structure. For example, "8–6–4" denotes a structural motif with eight-, six-, and four-membered rings. In addition, a superscript denotes the number of times each ring appears in the primitive unit cell, e.g., "$8-6^2-4$" refers to a unit cell with one eight-membered, two six-membered, and one four-membered ring. Each structure shown in Figure 2 was fully relaxed and the energies to form them from the hexagonal bilayer structure are provided on both a per Si atom basis for

DOI: 10.1021/acs.jpcc.6b07008
J. Phys. Chem. C 2016, 120, 26770−26781

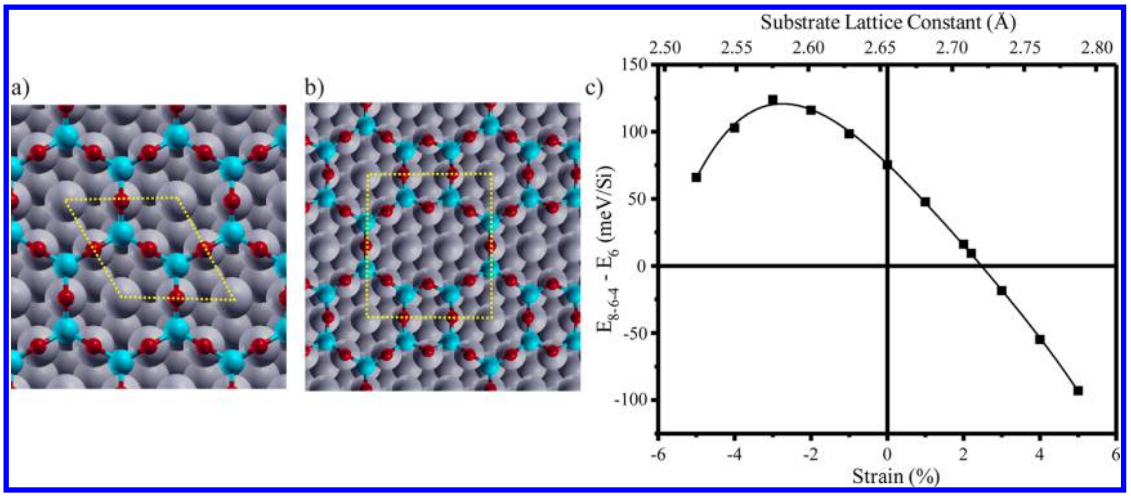

Figure 3. Models of commensurate (a) hexagonal and (b) 8−6−4 silica bilayers on a hexagonal metal substrate. The bilayers form (a) (2 × 2) and (b) $(3 \times 2\sqrt{3})$ overlayers. Cyan, red, and gray represent Si, O, and substrate atoms, respectively. The dashed lines highlight the unit cells. (c) Energy difference between the 8−6−4 and hexagonal structures as a function of biaxial strain induced in the hexagonal bilayer. The top axis provides the corresponding substrate lattice constant. Here, zero strain for the 8−6−4 structure does not denote a fully relaxed structure but rather a lattice match based on the lattice constant of the relaxed hexagonal bilayer.

uniformity and a per unit cell basis in Table 1, along with the areal densities of Si atoms. The data show energy variations on the order of hundreds of meV when the entire unit cells are considered. First, comparing the data on the per Si atom basis, one can see that all bilayer structures that deviate from hexagonal are higher in energy. Among these, the $8-5^2$ structure has the lowest energy, 17.8 meV/Si above the hexagonal structure, and 7^2-5^2 has the highest energy. Interestingly, adding the otherwise favored six-membered rings to the $8-5^2$ structure always increases the energy per Si atom. As illustrated in Figure 2, the hexagonal rings become highly distorted when eight-, six-, and five-membered rings mix, in particular in the $8-6^3-5^2$ structure, accounting for the high energy of these structures. The differences in energies of the bilayer structures stem primarily from structural distortions of the SiO_4 tetrahedra. In particular, the 7^2-5^2 structure includes in-plane O−Si−O bond angles that are reduced to 101.8° from 109.3° in the hexagonal bilayer. Similarly, large deviations of the Si−O−Si in-plane bond angles from a value typical of tetrahedral SiO_2-based materials,[16,43] which is about 140°, were observed for high energy structures. For instance, in the 7^2-5^2 structure some of the Si−O−Si bond angles (formed by atoms of five-membered rings) were reduced to 137°, and in the highly distorted $8-6^3-5^2$ structure some of the in-plane Si−O−Si bond angles were as low as 126°. It should be noted that the 7^2-5^2 and $8-6-5^2$ correspond to Haeckelite phases considered by Björkmann et al., who found identical energy differences between these structures and the hexagonal crystalline phase.[33]

The periodic boundary conditions imposed on the structures presented in Figure 2 and Table 1 make them crystalline 2D materials. Given these data, it is interesting to extract the amount of energy required to transform the hexagonal phase to each of the structures which can be thought of as a formation energy of the structure. This formation energy is given by the total energy of the structure per Si atom, referenced to the hexagonal bilayer, multiplied by the number of Si atoms in the unit cell; it is listed in Table 1 under the heading "ΔE_f, meV/unit cell". For the structures including six-membered rings, e.g., $8-6^n-4$, as n becomes large, the energies on this basis can be considered defect formation energies for non-six-membered rings in the hexagonal structure. Again, the smallest energy is observed for the $8-5^2$ ring combination, while the 7^2-5^2 and $8-6^3-5^2$ have the largest formation energies. More interestingly, although the calculated formation energy of the $8-5^2$ ring combination is low, this structure cannot be easily interfaced with six-membered ring structures. Therefore, the $8-5^2$ ring combination appears unlikely to occur as defects in the hexagonal bilayer; however, the low energy of the $8-5^2$ ring combination may make it possible to form extended $8-5^2$ crystalline domains. Meanwhile, 8−4 ring combinations become favored over 8−5 combinations when six-membered rings are introduced, making these motifs more favorable candidates for defects in hexagonal domains, in particular at anti-phase domain boundaries (APBs). The structures 8−6−4, $8-6^2-4$, and $8-6^3-4$, which can be labeled generally as $8-6^n-4$, contain such APBs (note that the APBs would be rotated 30° with respect to the close-packed direction of the hexagonal phase, as has been seen in experiments on 2D aluminosilicates[35]). For these structures, as n goes to infinity, the formation energy becomes the energy of a single APB (per eight-membered ring). The largest n in our calculations is 3, so the formation energy of the $8-6^3-4$ structure gives our best estimate for the energy cost of an APB, which is approximately 440 meV. At the same time, it is interesting to note that the defect formation energy increases as one adds more six-membered rings to the structure (by a smaller and smaller amount, consistent with expectations that the value will asymptote to the APB energy), suggesting that 8−4 ring combinations also prefer to phase-separate from six-membered rings.

Impact of Strain. Table 1 shows that the hexagonal structure has a high areal density. While this is not surprising, it suggests that tensile strain can be relieved by introducing different size rings into the hexagonal bilayer, thus providing an avenue to tune the structure. We first focus on biaxial strain. Consistent with experiments that reveal that the crystalline bilayer stretches to match twice the lattice constant of the late transition metals Ru and Pd,[4,5,11] we assume that the strain is dictated by the substrate, in this case a Ru(0001) surface.

DOI: 10.1021/acs.jpcc.6b07008
J. Phys. Chem. C 2016, 120, 26770−26781

The calculated hexagonal lattice parameter of Ru was a_{Ru} = 2.75 Å (1.6% larger than the experimental value), which is close to half the relaxed calculated and experimental hexagonal SiO_2 bilayer lattice constant of 5.30 Å.[10] Thus, forcing the in-plane lattice constant of hexagonal SiO_2 to match the Ru substrate produces a tensile strain of 3.6%. Similarly, among the structures shown in Figure 2, we selected a set that can be matched to a Ru substrate without substantial strain or the need to increase the size of the unit cell in the calculations. Figure 3a shows the commensurate (2×2) structure for the hexagonal motif, while Figure 3b illustrates that the 8−6−4 motif is confined to a $(3 \times 2\sqrt{3})$ structure. The 8−6^2−4 and 8−6^3−4 form $\begin{pmatrix} 5 & 2 \\ -3 & 2 \end{pmatrix}$ and $(5 \times 2\sqrt{3})$ overlayers, respectively. The total energies relative to the relaxed hexagonal bilayer for strained bilayer structures are shown under the heading "strained energy, meV/Si (biaxial strain)" in Table 1. We notice that the energies of the 8−6−4, 8−6^2−4, and 8−6^3−4 structures become smaller than the energy of the hexagonal bilayer structure; thus, it is concluded that tensile strain imparted by the substrate can make the formation of rings larger than six-membered thermodynamically favorable. Because the calculations overestimate the Ru lattice constant more than the bilayer SiO_2 lattice constant (see Supporting Information),[10] the aforementioned data correspond to greater tensile strain than is imparted experimentally. Therefore, additional calculations were performed on a subset of the structures at the experimental strain of 2.2%. As highlighted in Table 1, at this strain the energy of the 8−6^3−4 structure falls just below the hexagonal structure reinforcing the conclusion that strain can be relieved by introducing larger rings and that the density of the larger rings may be tuned through the strain. To gain more insight into how the energy to introduce 8−4 ring combinations into the hexagonal structure depends on strain, we also calculated the energy difference between the 8−6−4 structure and the hexagonal structure as a function of strain. The plot in Figure 3c shows that the 8−6−4 structure becomes favored as the tensile stress approaches 2.5% which corresponds to a substrate in-plane lattice constant of 2.72 Å; the plot also shows that very large compressive strains may also favor the 8−6−4 structure, although it is doubtful whether such large strains can be imparted by a substrate. Björkmann et al. also previously investigated the effect of strain on an 8−6−5^2 structure, and they too found that strain could reduce the energy below that of the hexagonal structure.[33] In their case, however, much larger strains were imposed, sufficient to increase the energy of the hexagonal structure by more than 600 meV.

Prior work showed that uniaxial strain energies in bilayer SiO_2 are much smaller than biaxial strain energies.[11] Such uniaxial strain may be applied through a nonhexagonal substrate, e.g., Pd(100) as in prior work,[11] or a hexagonal substrate since the weak bilayer−substrate van der Waals interactions do not impart an obviously large penalty to incommensuration along one direction. In both cases, the bilayer would be strained to match the substrate along one direction and allowed to relax along the orthogonal direction. To account for this possibility, we performed additional calculations on selected SiO_2 structures with enforced uniaxial strain. For each structure, we performed two relaxations with uniaxial strain imposed either parallel to or perpendicular to the edge of a six-membered ring. From these two calculations, the lowest energy result is reported in Table 1 for 3.6% and 2.2% strain. For the 8−6^n−4 structures, parallel strain produced lower energies while for the other structures perpendicular strain was favored. For the larger strain, the 8−6^3−4 structure is slightly lower in energy than the hexagonal structure, suggesting that the possibility to introduce eight-membered rings remains even if the strain is relieved uniaxially.

Doping with a Tetravalent Cation. Germanium was a natural choice to test as a tetravalent replacement for Si in the bilayer structures because of the following: Ge lies just below Si on the periodic table and behaves similarly; Ge forms stable tetrahedrally coordinated oxides including zeolitic structures;[42,44] and Ge-based zeolites exhibit a higher preference for double four-membered rings compared to Si-based materials.[45−47] We started by considering pure GeO_2 bilayers. With a hexagonal bilayer as a starting point and applying no symmetry constraints beyond restricting the material to a planar geometry, the material relaxed to the highly distorted structure pictured in Figure 4a. Unlike the SiO_2 bilayers, the

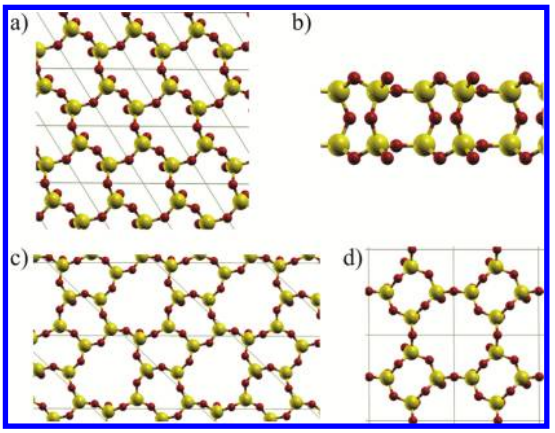

Figure 4. Models of relaxed GeO_2 bilayer structures: (a) top and (b) side views of a six-membered ring bilayer; (c) 8−5^2 structure; (d) 8−4 structure. The Ge−O−Ge bond angles that connect the two halves of the structures vary between 134.25° for the six-membered ring structure, 137.63° and 160.70° for the 8−5^2 structure, and 133.95° and 153.95° for the 8−4 structure. The non-180° angles make the central oxygen atoms visible in the top down views. Yellow and red balls represent Ge and O atoms, respectively. The lines highlight primitive unit cells.

structure does not adopt 180° bond T−O−T (where T is the tetrahedral atom Si or Ge) angles between the upper and lower planes. Although the T−O bond lengths increase from 1.63 to 1.79 Å in going from Si to Ge, the GeO_2 bilayer lattice constant is very close to that of the hexagonal SiO_2 bilayer (5.299 Å for GeO_2 versus 5.307 Å for SiO_2). The six-membered GeO_2 bilayer was calculated to be 116 meV/Ge higher in energy than the α-quartz phase, more than a factor of 2 larger than the analogous comparison for SiO_2. While this energy difference may not preclude formation of the bilayer when one considers that the bilayer intrinsically includes the surface energy which would significantly increase the energy of ultrathin GeO_2 in either the α-quartz or rutile bulk structures, the nonplanar outer oxygen layers would likely either decrease the van der Waals interactions with a metal substrate or distort to increase the interaction with the metal, in either case decreasing the driving force to form the bilayer. We also considered 8−5^2 and 8−4 GeO_2 bilayers with the resulting structures pictured in Figure 4b and Figure 4c, respectively. In both cases the layers are

DOI: 10.1021/acs.jpcc.6b07008
J. Phys. Chem. C 2016, 120, 26770−26781

highly distorted and higher in energy than the six-membered ring structure by 31 and 17 meV/Ge for the 8−5^2 and 8−4 structures, respectively. The reduction of the energy of the 8−4 structure below that of the 8−5^2 structure agrees with expectations based on differences between Si- and Ge-based zeolites.[45,46] Nonetheless, even if pure GeO_2 bilayers could be prepared, they offer no obvious advantage over the SiO_2 bilayers.

When Ge was partially substituted for Si in the bilayers, 180° bond angles between the upper and lower layers could be restored when Ge was always placed on opposite sides of the central oxygen plane from a Si atom. Similarly, in-plane distortions could be reduced by avoiding Ge−O−Ge connections. With these guidelines in mind, the series of six-membered and eight-membered ring structures pictured in Figure 5 were evaluated. For each structure, the Ge substitution energy was calculated based on the following reaction:

$$m\mathrm{SiO_2(h)} + \mathrm{GeO_2(q)} \rightarrow \mathrm{Si_{m-1}GeO_{2m}(b)} + \mathrm{SiO_2(q)} \quad (1)$$

where "h" refers to the hexagonal bilayer, "q" the α-quartz phase, and "b" a bilayer. The results are tabulated in Table 2. In all cases the energies are positive indicating that Ge substitution is energetically unfavorable. The lowest substitution energy, 153 meV/Ge, was obtained for a structure containing only six-membered rings; therefore, there was no indication that incorporating Ge into the bilayer can shift the equilibrium toward larger ring structures.

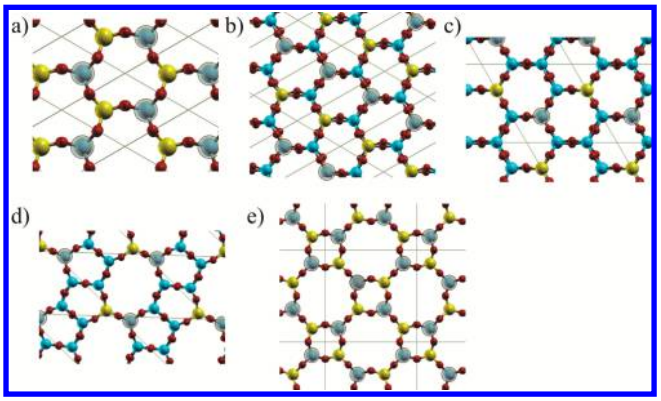

Figure 5. Models of $Si_{m-1}GeO_{2m}$ bilayer structures with Ge on both sides and no Ge−O−Ge bonds. Six-membered ring structures with (a) 50% Ge and a (1 × 1) unit cell; (b) 25% Ge substituted in a (2 × 1) pattern; and (c) 16.7% Ge substituted in a $(\sqrt{3} \times \sqrt{3})R30°$ pattern. Eight-membered ring structures with (d) 16.7% Ge substituted into in an 8−5^2 motif in a (1 × 1) unit cell and (e) 50% Ge substituted into an 8−4 motif with a $c(2 \times 2)$ pattern. Color scheme same as in Figures 1 and 4. Lines indicate primitive unit cells, and shaded circles highlight Si atoms above Ge atoms in the bottom layer.

Table 2. Computed Ge Substitution Energies (ΔE) for a Series of $Si_{m-1}GeO_{2m}$ Bilayers[a]

motif	supercell	m	lattice constants a (Å), b (Å), α (deg)	ΔE (meV/Ge)
6	1 × 1	2	5.37, 5.37, 120	153
6	2 × 1	4	5.33, 10.68, 119.9	201
6	$(\sqrt{3} \times \sqrt{3})R30°$	6	9.27, 9.27, 120	198
8−4	$c(2 \times 2)$	2	10.60, 10.60, 90	194
8−5^2	1 × 1	6	10.67, 10.68, 137.1	229

[a]The "motif" column gives the ring sizes using the nomenclature described in the text, and "supercell" refers to the size of the Ge-substituted cell (before relaxation) with respect to the unit cell of the corresponding pure SiO_2 bilayer structure.

Doping with a Trivalent Cation. Substituting trivalent cations for Si in SiO_2 leads to a wide range of silicate structures and can create catalytically interesting materials.[16,32] Because replacing tetravalent Si with a trivalent cation creates an electron deficit, extra-framework electron donors must accompany the trivalent cations. The catalytic activity may be associated with the trivalent cation directly or with the electron donor.[32] Here, we consider Al as the trivalent cation, since it is the most common tetrahedral substituent in zeolites and other silicates. For most of the work presented here, K was used as the electron donor. Although K does not form the Brønsted acid sites often of interest in zeolite catalysis that the seemingly simpler H does, we found that the short O−H bonds created structural distortions that made the energetics of the structures sensitive to the precise placement of the H atoms. With four potential locations for the O−H group for each Al, the number of structures that need to be considered becomes large. In contrast, we find that the larger K ion prefers to sit nearly above the centers of the rings and the minimum energy location can be easily found. The position above the center of the ring is consistent with a prior theoretical investigation of alkaline and alkaline earth metal adsorption on undoped 2D silica.[48] Also, with K as the electron donor, the Al-substituted structures were far less distorted suggesting that for K, the differences in energies between different Al-substituted structures reflect the impact of the Al. In considering Al-substituted structures, Lowenstein's rule, which prohibits adjacent trivalent cations in a corner-sharing tetrahedral network, was followed.[20,49]

Substituting Al for Si in six-membered ring bilayers was studied as a function of Al concentration for Al placed on one side of the bilayer and for equal amounts of Al placed on both sides. Several representative Al-substituted structures are depicted in Figure 6. Although incorporating the larger Al

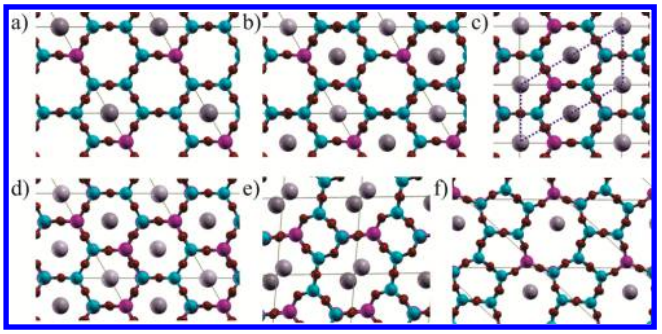

Figure 6. Models of a series of representative $Si_{m-1}AlO_{2m}K$ structures: (a) m = 12 with Al substituted on one side in a $(\sqrt{3} \times \sqrt{3})R30°$ pattern; (b) m = 6 with Al substituted on both sides in a $(\sqrt{3} \times \sqrt{3})R30°$ pattern; (c) m = 4 with Al substituted on both sides in a (2 × 1) pattern; (d) m = 3 with Al substituted on both sides in a $(\sqrt{3} \times \sqrt{3})R30°$ pattern; (e) m = 4 with Al substituted on both sides in an 8−4 motif; (f) m = 6 with Al substituted on both sides in an 8−5^2 motif. Magenta, gray, cyan, and red balls represent Al, K, Si, and O atoms, respectively. Lighter gray highlights K atoms above the top of the bilayer and darker gray K atoms beneath the lower layer. The solid lines indicate unit cells; in (c) the dashed line indicates an alternate (2 × 1) unit cell with the same number of atoms as the rectangular unit cell.

DOI: 10.1021/acs.jpcc.6b07008
J. Phys. Chem. C 2016, 120, 26770−26781

cation into the framework expands the spacing between six-membered rings by up to 3.5% for 50% Al substitution, comparing the structures in which Al was substituted for Si in a $(\sqrt{3} \times \sqrt{3})R30°$ pattern (Figure 6a Al on one side and Figure 6b Al on both sides) shows that Al does not significantly distort the hexagonal structure (with K as the electron donor) and all the bonds connecting the two layers remain near 180°. As expected for the larger Al^{3+} cation, the Al−O bonds are longer than the Si−O bonds: 1.77 Å for the bonds between Al and the O atoms in the top and bottom planes of the bilayer (outer oxygens) and 1.72 Å for the 180° bonds connecting the two layers. Meanwhile, Si bonds to O shared with Al are slightly shortened to 1.61 Å while the remaining Si−O bonds to outer oxygens of adjacent SiO_4 tetrahedra are slightly lengthened to 1.64−1.65 Å. The Al−O−Si distance across the 180° bond is larger than the neighboring Si−O−Si interplanar spacing: 3.31 Å versus 3.26 Å. A flattening of the Al−O−Si bond angles in the outer oxygen layers, however, left the uppermost and lowermost oxygen atoms in the bilayers nearly coplanar. The above numbers are for Al on one side; they change very little when Al is incorporated on both sides. The distortions are also minimal for the (2×1) substitution with the rectangular unit cell in Figure 6d. Note that the K ions may occupy different rings in these structures, and different registries between the Al on opposite sides of the bilayer are possible for the two-sided structures. Figure 6 shows the lowest energy arrangements of the K and Al ions that we found. In the work presented below, only minimum energy K and Al configurations are considered.

The energy to substitute Al for Si was calculated based on the following reaction:

$$m\mathrm{SiO_2(b)} + \frac{1}{2}\mathrm{Al_2O_3(c)} + \frac{1}{2}\mathrm{K_2O(af)} \rightarrow \mathrm{Si_{m-1}AlO_{2m}K(b)} + \mathrm{SiO_2(q)} \quad (2)$$

where "b" indicates a bilayer, "c" the corundum structure, "af" the antifluorite structure, and "q" the α-quartz structure. The results are plotted in Figure 7 as a function of m for six-membered ring structures with Al. In all cases, the reaction is very favorable by ~2 eV. The results also show a strong preference for substituting equal amounts of Al on both sides, which may be related to equilibrating the stress of incorporating the larger Al^{3+} cation on both sides. The curves appear nonmonotonic at first glance, but two factors must be considered. First, excluding $m = 2$ where only one substitution pattern is possible which yields a (1×1) unit cell when possible longer range rumpling of the bilayer is excluded, the lower energy structures are rotated 30° from the hexagonal pure silica bilayer, suggesting that strain is more efficiently accommodated when the unit cell is rotated. Second, the $m = 4$ and 8 structures for Al on both sides (and the $m = 8$ and 16 for Al on one side) can be produced through lower energy linear combinations of $R30°$ structures, thereby producing a monotonically decreasing curve. The end result is a repulsive Al−Al interaction that decreases the favorability of the substitution reaction as the Al content increases.

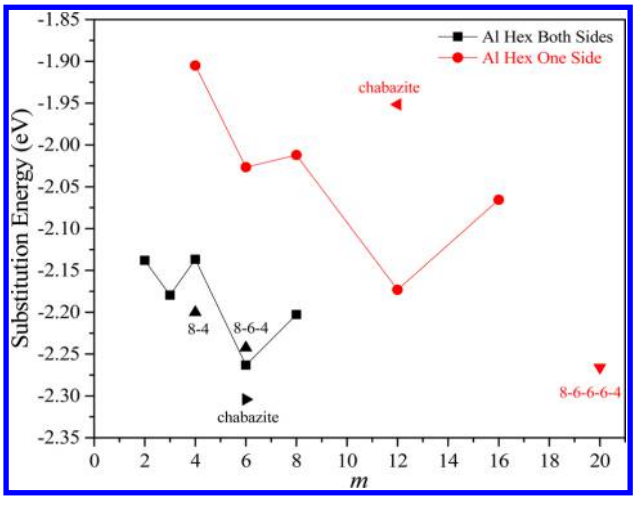

Figure 7. Plot of the energy to substitute Al into bilayer silica to form $Si_{m-1}AlO_{2m}K$ as a function of Al concentration. The lines connect points for six-membered ring structures, while the labels indicate points for different bilayer motifs and a zeolite. Red highlights data for Al on one side of the double ring structure and black on both sides.

Figure 7 also includes data for different bilayer structures and for chabazite, a zeolite that shares structural features with the bilayers.[35,50] As shown in Figure 8a, the chabazite unit cell can be pictured as including double six-membered rings; replicating this unit cell in three dimensions introduces eight-membered rings. In its pure silica form, calculations indicate that chabazite is 42 meV/Si higher in energy than α-quartz and 8 meV/Si lower in energy than the hexagonal bilayer. Comparing the energy to insert one Al and two Al on opposite sides of the double six-membered rings (Figure 8b) in chabazite reveals substitution energies in the same range as the bilayer (the energies were calculated using reaction 2 except with the chabazite structure substituting for the bilayer). More significantly, the results show that it is also substantially more favorable to incorporate Al into both six-membered rings in the chabazite unit cell, indicating that this feature is not unique to bilayers.

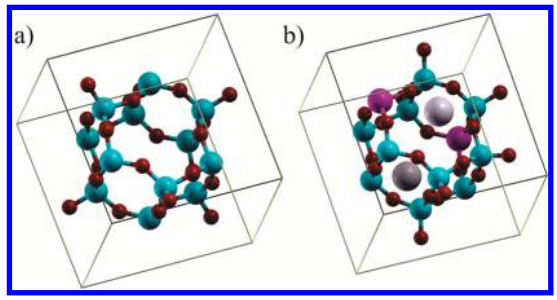

Figure 8. Models of the unit cell of the zeolite chabazite highlighting the double six-membered ring feature: (a) pure silica and (b) $^1/_6$ of the Si replaced by Al with K as the electron donor. Color scheme is as in Figure 5 with depth cueing so that atoms deeper into the page appear darker.

The plot in Figure 7 also includes several structures with eight-membered rings where the substitution energies are very close to the six-membered ring structures at the same Al concentrations. For these cases, the substitution energies were calculated by taking the corresponding pure silica bilayer on the left side of reaction 2. The substitution energy for the 8−4 structure with $^1/_4$ Al appears more favorable than the six-membered ring structure at the same Al concentration. However, a lower energy $^1/_4$ Al six-membered ring structure can be created by adding two unit cells of the $^1/_3$ Al with one unit cell of the $^1/_6$ Al six-membered ring structures. Finally, the most favorable substitution energy was found for an $8-6^3-4$

DOI: 10.1021/acs.jpcc.6b07008
J. Phys. Chem. C 2016, 120, 26770−26781

structure with m = 20 even though Al on just one side was considered.

As with the pure silica structures, it is useful to consider the energy required to transform six-membered ring $Si_{m-1}AlO_{2m}K$ structures into motifs containing eight-membered rings. These formation energies are summarized in Table 3. For these

Table 3. Computed Energies (ΔE_{SiAl}) To Convert a Hexagonal $Si_{m-1}AlO_{2m}X$ (X = K, H) Bilayer into the Listed Structural Motif[a]

motif	M	electron donor	ΔE_{SiAl} (meV)	$\Delta E_{SiAl} - \Delta E_{Si}$ (meV)
8−4	4	K	306	16
8−4	4	H	290	0
$8-5^2$	6	K	336	142
8−6−4	6	K	401	42

[a]The rightmost column provides the difference between these formation energies for Al-doped and pure SiO_2 bilayers.

calculations, Al was placed on both sides of the bilayer, and the formation energies were compared with those for pure silica structures calculated with the NABF basis which yields slightly different values than those presented in Table 3 (by ∼20 meV/unit cell for the formation energy of the 8−4 structure) but follow the same trends. In any case, it is clear that Al substitution does not change the favorability of six-membered ring structures and that a similar conclusion would likely be drawn if H were used instead of K as the electron donor. In comparing the formation energies for pure and Al-doped structures, a noteworthy feature is that only the $8-5^2$ motif shows a large difference from pure SiO_2, becoming energetically unfavorable compared to the 8−4 motif, despite the higher Al concentration in the latter. This trend is consistent with the experimental observation of many more 8−4 versus 8−5 ring combinations when Al is introduced into the bilayer.[35]

In a search for the lowest energy Al-doped eight-membered ring structures, the Al was found to prefer locations adjoining eight-membered rings with either K or H above the eight-membered ring. As illustrated in Figure 9, for the 8−6−4 motif

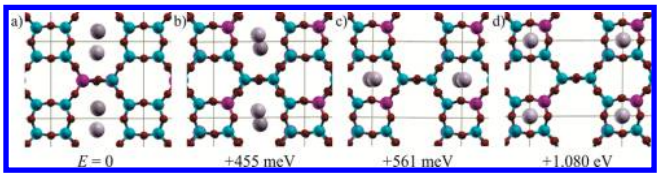

Figure 9. Comparison of the energetics of $Si_5AlO_{12}K$ in an 8−6−4 motif with Al on both sides and the Al and K in different sites. (a) The lowest energy structure with Al at the vertex between two eight- and one six-membered ring, and the K above the eight-membered ring. (b−d) With the Al at the vertex of four-, six-, and eight-membered rings, the differences between putting the K above the different size rings can be compared. All energies are referenced to the minimum energy structure in (a) and are on a per unit cell basis. Color scheme is as in Figure 6.

with Al on both sides, the minimum energy structure in Figure 9a has both Al at the vertices between an eight-membered and two six-membered rings (an 8−6−6 vertex) with K in the eight-membered ring. To assess the impact of the K placement on the energetics, we compared structures with the Al at an 8−6−4 vertex which allows the K to be located above the four-, six-, or eight-membered ring as pictured in Figure 9b−d. Placing the K above the eight-membered ring was 106 and 519 meV/unit cell more favorable than above the six- and four-membered rings, respectively, suggesting that the preference for Al to locate adjacent to eight-membered rings is in fact driven by the preference for the electron donor to occupy sites in the eight-membered rings (at least for K and H). These conclusions were reinforced by comparing a series of Al-substituted $8-6^3-4$ structures which allow a variety of Al sites; in this case Al was restricted to one side of the bilayer. The lowest energy structure (Figure 10a) has the Al at an 8−6−4 vertex with K near the

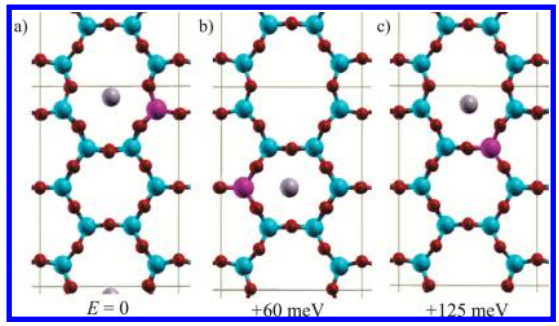

Figure 10. Comparison of the energetics of $Si_{19}AlO_{40}K$ with Al on one side as a function of the location of the Al and K atoms. (a) Minimum energy structure with Al at the vertex between four-, six-, and eight-membered rings with the K above the eight-membered ring. (b) The next lowest energy structure has Al at the vertex between three six-membered rings and K above a six-membered ring. (c) Aluminum at the vertex between two six- and one eight-membered ring and the K above the eight-membered ring. The energies are on a per unit cell basis and are referenced to the minimum energy structure in (a).

center of the eight-membered ring. Interestingly, the next lowest energy structure (Figure 10b), by 60 meV, has the Al at a 6−6−6 vertex which restricts the K to a six-membered ring, which in turn is 65 meV more favorable than placing the Al at an 8−6−6 vertex with K above the eight-membered ring. Thus, despite the preference for K to occupy eight-membered rings, by an estimated 106 meV (Figure 9c), the energy difference between Al adjacent to all six-membered rings and next to an eight-membered ring is smaller, only 60 meV. Therefore, the Al does not appear to show a preference for larger rings; rather it is the ability to locate the electron donor in a larger ring that carries the Al with it to sites along the larger rings. This suggests that finding electron donors with a stronger preference for larger rings than H or K may make eight-membered ring motifs favorable over hexagonal structures.

DISCUSSION

The energetics of a range of SiO_2 bilayer structures with different size rings of corner-sharing SiO_4 tetrahedra were evaluated, and while it was found that many of these were close in energy, a hexagonal structure was lowest in energy. On the basis of the observation that introducing different size rings into the bilayer decreases the density, it was surmised that tensile strain could make motifs incorporating eight-membered rings favored over purely hexagonal structures. Calculations showed that indeed both biaxial and uniaxial strain could shift the balance toward eight-membered ring structures. These findings are supported by prior experimental observations. First, the small energy differences between the structural motifs are consistent with the observation of amorphous bilayers on Ru(0001), Pt(111), and Pd(100) substrates with four- through nine-membered rings.[6,12,36] Moreover, crystalline bilayers on

DOI: 10.1021/acs.jpcc.6b07008
J. Phys. Chem. C 2016, 120, 26770−26781

Ru(0001) and Pd(100) are found to stretch to match twice the lattice constants of the metal surfaces.[4,7,11] For Pd(100) where the tensile strain is 3.9%, nearly periodic arrays of APBs with elongated rings are seen that can help accommodate the strain.[11] For Ru(0001) with 2.2% tensile strain, the APB density is much lower, but it is difficult to determine whether these APBs are thermodynamically driven or a result of merging nuclei.[4,19,51] The observation of 8−5 ring combinations, which we found do not interface well with six-membered rings but may accommodate merging growth fronts better than 8−4 combinations in certain cases, argues for the merging nuclei scenario.[51] On the other hand, less dense amorphous bilayer domains are always seen together with hexagonal crystalline bilayers on Ru(0001) which can also reduce strain.[5,51]

The above suggests that tensile lattice strain can be a viable method to control the structure of silica bilayers. Alloys of late transition metals that form solid solutions, e.g., Rh−Ni and Pd−Ni, can be used to tune the strain.[52,53] Because the bilayer interactions with late transition metal surfaces are of van der Waals type, the exact choice of metal should not matter. Still, there are limitations to how much lattice strain can be imparted. For Pt(111) where a hexagonal bilayer would be strained by 4.6%, only amorphous bilayers have been seen.[36] Thus, above a certain lattice mismatch, an amorphous structure becomes favored over hexagonal bilayers, even with different size rings incorporated.

Precisely controlling the silica coverage just below the ideal coverage for a hexagonal bilayer can also provide a route to imposing tensile strain. Formation of the closed bilayer can be understood in terms of surface and interfacial energy minimization. The lack of any dangling bonds minimizes the surface and interfacial interactions of the silica film, while expanding the bilayer to cover as much of the high surface energy metal substrate as possible reduces the metal's surface energy. Because the hexagonal structure is the densest, at silica coverages just below the ideal hexagonal bilayer coverage, the energy may be reduced by introducing different size rings which reduce the density and therefore allow greater coverage of the metal substrate. On the basis of Table 3, a 1.8% lower coverage could be accommodated by a transition to an $8-6^3-4$ structure, while a greater deviation could most likely be accommodated by amorphous domains. This suggests that part of the difficulty with obtaining solely crystalline films may stem from an inability to adequately control the silica coverage. The challenge of controlling the silica coverage is exacerbated by the propensity of zerovalent Si to migrate into late transition metals[54−56] and by the high temperature bilayer preparation conditions where the O_2 pressure must be high enough to avoid SiO_2 decomposition but not high enough to oxidize the metal substrate. For Ru(0001), a $SiO_{2.5}$ monolayer with O−Ru bonds forms when the silica coverage is significantly below that required to form a closed bilayer,[7] while on Pt(111) no monolayer phase exists and lower silica coverages produce an amorphous bilayer partially covering the surface.[36] Thus, the ability to use the silica coverage to tune the bilayer structure can depend on the substrate choice.

Substituting Ge for Si in the bilayer would appear to be a promising route (i) to increasing the size of the openings in the hexagonal structure, since Ge−O bonds are longer than Si−O bonds, and (ii) to introducing different size rings because Ge-based zeolites exhibit a propensity to include double four-membered rings.[45−47] However, no advantage was found to substituting Ge for Si. The underlying reason for the difficulty in forming GeO_2 based bilayers was the much larger energy penalty of forming 180° Ge−O−Ge interlayer bonds (compared to SiO_2) which resulted in highly distorted bilayers. This agrees with prior theoretical investigations of SiO_2 and GeO_2 tetrahedral structures that found a much deeper and more symmetric energy minimum near the favored Ge−O−Ge bond angle; while the cost to straighten Si−O−Si bond angles to 180° was very small, ∼10 meV/Si for Si versus ∼100 meV/Ge for Ge.[57] While some of these issues could be resolved with Ge−O−Si interlayer bonds, mixed $Si_{1-x}Ge_xO_2$ did not have larger hexagonal openings than SiO_2 hexagonal bilayers and showed no greater propensity to form larger rings. We now argue that other tetravalent substituents are not more promising. Continuing down the periodic table, the larger Sn^{4+} cation only forms octahedrally coordinated pure oxides, suggesting that a SnO_2 tetrahedral bilayer would be even less favorable than GeO_2. Regarding the transition metals, based on crystal radii (the smallest crystal radii favor tetrahedral coordination), the most promising to form tetravalent states compatible with tetrahedral coordination would be Ti, Cr, and Mn.[58,59] Attempts to synthesize a mixed $Si_{1-x}Ti_xO_2$ tetrahedral bilayer instead produced a structure with a Ti oxide layer bound to the metal substrate overlaid by a Si oxide layer.[60] The challenge with Ti is that it easily forms oxide layers strongly bound to a number of transition metal surfaces.[61−63] This stems from the weaker Ti−O bonds, compared to Si−O, which are closer in strength to the metal oxygen bonds on late transition metal surfaces. This challenge is expected to be more severe for the more easily reducible Cr^{4+} and Mn^{4+} cations, indicating that it will be very difficult to prepare bilayer Si with tetravalent transition metal cation substituents through a high temperature process on late transition metals.

In contrast to the tetravalent cations, our calculations indicate that trivalent Al can readily substitute for Si in the bilayer with minimal distortion. Furthermore, we find that the energetics of Al substitution are very similar for the two-dimensional bilayer and the three-dimensional zeolite chabazite. Although the Al−O bonds are significantly longer than the Si−O bonds in pure silica, the shortening of the Si−O bonds adjacent to Al and a flattening of the O−Al−O bond angles compensate for the longer Al−O bonds without appreciably changing the structure. Thus, in accord with experimental observations, we find that Al substitutes as readily for Si in the two-dimensional bilayer as it does in zeolites.[8,20,35,64] Experiments have revealed a high density of 8−4 APBs as well as a broadening of the ring size distribution in amorphous bilayers at Al concentrations above 25%.[20,35,64] In contrast, we found only small differences between the energies required to form larger ring structures in Al-doped versus pure SiO_2 bilayers. Still, if larger rings are introduced, by lattice strain for example, we find that Al prefers to occupy sites adjacent to the larger rings. Interestingly, this preference is driven not by an ability to more easily accommodate Al-induced strain at the larger rings but by a preference for the electron donors, H and K in this study, that accompany Al to sit above the larger rings. This suggests that searching for electron donors with a greater preference for the larger rings can be a fruitful path to inducing larger rings to form. It should be noted that the transition metal substrate can also donate the electrons needed to fill the Al−O−Si bonding orbitals, which would create chemical and dipolar interactions between the metal and the bilayer.[48] As no electron donors were explicitly deposited with the Al in prior experimental studies and because hydrogen desorbs from Si−Al

DOI: 10.1021/acs.jpcc.6b07008
J. Phys. Chem. C 2016, 120, 26770−26781

bilayers well below the bilayer formation temperature,[21] it can be assumed that the metal substrate donated the necessary electrons in those experiments. In this case a chemical interaction with the oxygens adjacent to the Al and the substrate would be expected, leading to a preference for the Al to occupy sites closest to the metal as has been observed experimentally.[20] The chemical interaction with the substrate near Al sites would also be expected to reduce the bilayer−substrate separation near Al sites which would cause a rumpling of the bilayer at low Al concentrations that could be avoided by phase separation into Al-rich domains.[20] Therefore, some of the differences between experiment and theory can be related to how the electron deficit was accommodated when the mixed Si−Al organized into bilayers. This suggests future directions for both experiment and modeling. On the modeling side, performing calculations with the metal substrate would undoubtedly better mimic the experiments carried out to date; Schlexer et al. have made progress along this direction.[48] On the other hand, our calculations indicate that co-depositing an electron donor with the Al and Si may allow control over the bilayer structure independent of the metal substrate. Strongly electropositive alkalis and alkaline earths would be obvious candidates because they more readily donate electrons than the late transition metal substrates, are commonly found and used in natural and synthetic zeolites,[32] and readily ionize on late transition metal surfaces.[65] Schlexer et al. predict that the alkalis will intercalate at the interface between the 2D aluminosilicate and Ru(0001), providing support for this approach.[48]

SUMMARY

Density functional theory was used to investigate pathways to controlling the structure of two-dimensional silica. For pure SiO_2, a hexagonal bilayer comprising mirror image planes of corner-sharing SiO_4 tetrahedra arranged in six-membered rings was found to be as little as 44 meV/Si higher in energy than α-quartz. A series of similar bilayer structural motifs including four- through eight-membered rings of corner-sharing tetrahedra were found to be only slightly higher in energy than the hexagonal bilayer, consistent with experimental observations of an amorphous bilayer that includes such features. The lowest energy hexagonal phase was also found to be the densest, suggesting that tensile strain can be relieved by incorporating different size rings into the hexagonal phase. Calculations supported this view. A 3.6% uniaxial or biaxial strain was sufficient to reduce the energy of structures with eight-, six-, and four-membered rings below that of structures with only six-membered rings. A smaller 2.2% biaxial strain also favored the introduction of eight- and four-membered rings. These findings are consistent with experiments that revealed either coexisting less-dense amorphous phases or nearly periodic arrays of larger rings when hexagonal bilayers were stretched to match the lattice of a transition metal support.[5,11] They also highlight the potential to control the structure by tuning the lattice mismatch.

The ability to control the structure by replacing Si with tetravalent and trivalent atoms was also investigated. The large penalty incurred by 180° Ge−O−Ge bonds precluded the formation of a GeO_2 hexagonal bilayer analogous to the SiO_2 bilayer. This issue could be circumvented by avoiding Ge−O−Ge bonds in a mixed $Si_{m-1}GeO_{2m}$ bilayer, but the formation of such bilayers was energetically unfavorable and the mixed bilayers showed no greater propensity to form non-six-membered rings than pure bilayer SiO_2. On the other hand, substituting trivalent Al for Si was energetically favorable and only minimally distorted the bilayer structure. With extra-framework K and H supplying electrons to fill the bonding states of the $Si_{m-1}AlO_{2m}$ bilayer, the favorability of six-membered rings was not appreciably altered. On the other hand, Al favored sites adjacent to eight-membered rings when these were present, a preference driven by the ability to place the extra-framework K or H in the larger ring. This suggests that finding electron donors that favor the larger rings by more than the cost of Si−O−Si bond distortions that the larger rings introduce will be a fruitful path toward achieving structural control over bilayer silicate structures.

ASSOCIATED CONTENT

Supporting Information

The Supporting Information is available free of charge on the ACS Publications website at DOI: 10.1021/acs.jpcc.6b07008.

Benchmarking calculations and results (PDF)

AUTHOR INFORMATION

Corresponding Author

*E-mail: eric.altman@yale.edu.

Notes

The authors declare no competing financial interest.

ACKNOWLEDGMENTS

This project was supported by the National Science Foundation through Grant DMR 1506800. Initial work by AM on SiO_2 bilayers was supported by National Science Foundation Grant DMR 1119826, which supports the Center for Research on Interface Structures and Phenomena, the Yale Materials Research Science and Engineering Center. E.I.A. acknowledges partial support of the work on Al doping by the Department of Energy through Basic Energy Sciences Grant DE-SC0014414.

REFERENCES

(1) Geim, A. K. Nobel Lecture: Random Walk to Graphene. *Rev. Mod. Phys.* **2011**, *83*, 851−862.
(2) Novoselov, K. S. Nobel Lecture: Graphene: Materials in the Flatland. *Rev. Mod. Phys.* **2011**, *83*, 837−849.
(3) Xu, M.; Liang, T.; Shi, M.; Chen, H. Graphene-Like Two-Dimensional Materials. *Chem. Rev.* **2013**, *113*, 3766−3798.
(4) Loffler, D.; Uhlrich, J. J.; Baron, M.; Yang, B.; Yu, X.; Lichtenstein, L.; Heinke, L.; Buchner, C.; Heyde, M.; Shaikhutdinov, S.; et al. Growth and Structure of Crystalline Silica Sheet on Ru(0001). *Phys. Rev. Lett.* **2010**, *105*, 146104.
(5) Heyde, M.; Shaikhutdinov, S.; Freund, H. J. Two-dimensional Silica: Crystalline and Vitreous. *Chem. Phys. Lett.* **2012**, *550*, 1−7.
(6) Lichtenstein, L.; Buchner, C.; Yang, B.; Shaikhutdinov, S.; Heyde, M.; Sierka, M.; Wlodarczyk, R.; Sauer, J.; Freund, H. J. The Atomic Structure of a Metal-supported Vitreous Thin Silica Film. *Angew. Chem., Int. Ed.* **2012**, *51*, 404−7.
(7) Yang, B.; Kaden, W. E.; Yu, X.; Boscoboinik, J. A.; Martynova, Y.; Lichtenstein, L.; Heyde, M.; Sterrer, M.; Wlodarczyk, R.; Sierka, M.; et al. Thin Silica Films on Ru(0001): Monolayer, Bilayer and Three-dimensional Networks of [SiO_4] Tetrahedra. *Phys. Chem. Chem. Phys.* **2012**, *14*, 11344−11351.
(8) Boscoboinik, J. A.; Yu, X.; Yang, B.; Fischer, F. D.; Wlodarczyk, R.; Sierka, M.; Shaikhutdinov, S.; Sauer, J.; Freund, H.-J. Modeling Zeolites with Metal-Supported Two-Dimensional Aluminosilicate Films. *Angew. Chem., Int. Ed.* **2012**, *51*, 6005−6008.
(9) Huang, P. Y.; Kurasch, S.; Alden, J. S.; Shekhawat, A.; Alemi, A. A.; McEuen, P. L.; Sethna, J. P.; Kaiser, U.; Muller, D. A. Imaging

DOI: 10.1021/acs.jpcc.6b07008
J. Phys. Chem. C 2016, 120, 26770−26781

Atomic Rearrangements in Two-Dimensional Silica Glass: Watching Silica's Dance. *Science* **2013**, *342*, 224−227.
(10) Huang, P. Y.; Kurasch, S.; Srivastava, A.; Skakalova, V.; Kotakoski, J.; Krasheninnikov, A. V.; Hovden, R.; Mao, Q.; Meyer, J. C.; Smet, J.; et al. Direct Imaging of a Two-Dimensional Silica Glass on Graphene. *Nano Lett.* **2012**, *12*, 1081−1086.
(11) Altman, E. I.; Götzen, J.; Samudrala, N.; Schwarz, U. D. Growth and Characterization of Crystalline Silica Films on Pd(100). *J. Phys. Chem. C* **2013**, *117*, 26144.
(12) Altman, E. I.; Schwarz, U. D. Structural and Electronic Heterogeneity of Two Dimensional Amorphous Silica Layers. *Adv. Mater. Interfaces* **2014**, *1*, 1400108.
(13) Artyukhov, V. I.; Chernozatonskii, L. A. Theoretical Study of Two-Dimensional Silica Films. *J. Phys. Chem. C* **2010**, *114*, 9678−9684.
(14) Wang, G.; Loh, G. C.; Pandey, R.; Karna, S. P. Novel Two-Dimensional Silica Monolayers with Tetrahedral and Octahedral Configurations. *J. Phys. Chem. C* **2015**, *119*, 15654−15660.
(15) Geim, A. K.; Grigorieva, I. V. Van der Waals heterostructures. *Nature* **2013**, *499*, 419−425.
(16) Griffen, D. T. *Silicate Crystal Chemistry*; Oxford University Press: New York, 1992.
(17) Emmez, E.; Yang, B.; Shaikhutdinov, S.; Freund, H.-J. Permeation of a Single-Layer SiO_2 Membrane and Chemistry in Confined Space. *J. Phys. Chem. C* **2014**, *118*, 29034−29042.
(18) Altman, E. I.; Schwarz, U. D. Structural and Electronic Heterogeneity of Two Dimensional Amorphous Silica Layers. *Adv. Mater. Interfaces* **2014**, *1*, 1400108.
(19) Shaikhutdinov, S.; Freund, H.-J. Ultrathin Silica Films on Metals: The Long and Winding Road to Understanding the Atomic Structure. *Adv. Mater.* **2013**, *25*, 49−67.
(20) Boscoboinik, J. A.; Shaikhutdinov, S. Exploring Zeolite Chemistry with the Tools of Surface Science: Challenges, Opportunities, and Limitations. *Catal. Lett.* **2014**, *144*, 1987−1995.
(21) Boscoboinik, J. A.; Yu, X.; Emmez, E.; Yang, B.; Shaikhutdinov, S.; Fischer, F. D.; Sauer, J.; Freund, H.-J. Interaction of Probe Molecules with Bridging Hydroxyls of Two-dimensional Zeolites: A Surface Science Approach. *J. Phys. Chem. C* **2013**, *117*, 13547−13556.
(22) Sauer, J. Bronsted Activity of Two-dimensional Zeolites Compared to Bulk Materials. *Faraday Discuss.* **2016**, *188*, 227−234.
(23) Büchner, C.; Lichtenstein, L.; Stuckenholz, S.; Heyde, M.; Ringleb, F.; Sterrer, M.; Kaden, W. E.; Giordano, L.; Pacchioni, G.; Freund, H.-J. Adsorption of Au and Pd on Ruthenium-Supported Bilayer Silica. *J. Phys. Chem. C* **2014**, *118*, 20959−20969.
(24) Ulrich, S.; Nilius, N.; Freund, H.-J.; Martinez, U.; Giordano, L.; Pacchioni, G. Realization of an Atomic Sieve: Silica on Mo(1 1 2). *Surf. Sci.* **2009**, *603*, 1145−1149.
(25) Breck, D. W. *Molecular Sieves: Structure, Chemistry and Use*; John Wiley & Sons: New York, 1974.
(26) Kulprathipanja, S. *Zeolites in Industrial Separation and Catalysis*; Wiley-VCH Verlag: Weinheim, Germany, 2010.
(27) Mehio, N.; Dai, S.; Jiang, D.-e. Quantum Mechanical Basis for Kinetic Diameters of Small Gaseous Molecules. *J. Phys. Chem. A* **2014**, *118*, 1150−1154.
(28) Emmez, E.; Yang, B.; Shaikhutdinov, S.; Freund, H.-J. Permeation of a Single-Layer SiO2 Membrane and Chemistry in Confined Space. *J. Phys. Chem. C* **2014**, *118*, 29034−29042.
(29) Włodarczyk, R.; Sierka, M.; Sauer, J.; Löffler, D.; Uhlrich, J.; Yu, X.; Yang, B.; Groot, I.; Shaikhutdinov, S.; Freund, H. J. Tuning the Electronic Structure of Ultrathin Crystalline Silica films on Ru(0001). *Phys. Rev. B: Condens. Matter Mater. Phys.* **2012**, *85*, 085403.
(30) Zhong, J.-Q.; Kestell, J.; Waluyo, I.; Wilkins, S.; Mazzoli, C.; Barbour, A.; Kaznatcheev, K.; Shete, M.; Tsapatsis, M.; Boscoboinik, J. A. Oxidation and Reduction under Cover: Chemistry at the Confined Space between Ultrathin Nanoporous Silicates and Ru(0001). *J. Phys. Chem. C* **2016**, *120*, 8240−8245.
(31) Arruebo, M.; Mallada, R.; Pina, M. P. Zeolite Membranes. In *Handbook of Membrane Separations*; CRC Press: Boca Raton, FL, 2008; pp 269−323.
(32) Auerbach, S. M.; Carrado, K. A.; Dutta, P. K. *Handbook of Zeolite Science and Technology*; M. Dekker: New York, 2003.
(33) Björkman, T.; Kurasch, S.; Lehtinen, O.; Kotakoski, J.; Yazyev, O. V.; Srivastava, A.; Skakalova, V.; Smet, J. H.; Kaiser, U.; Krasheninnikov, A. V. Defects in Bilayer Silica and Graphene: Common Trends in Diverse Hexagonal Two-Dimensional Systems. *Sci. Rep.* **2013**, *3*, 3482.
(34) Altman, E. I.; Götzen, J.; Samudrala, N.; Schwarz, U. D. Growth and Characterization of Crystalline Silica Films on Pd(100). *J. Phys. Chem. C* **2013**, *117*, 26144−26155.
(35) Boscoboinik, J. A.; Yu, X.; Yang, B.; Shaikhutdinov, S.; Freund, H.-J. Building Blocks of Zeolites on an Aluminosilicate Ultra-thin Film. *Microporous Mesoporous Mater.* **2013**, *165*, 158−162.
(36) Yu, X.; Yang, B.; Boscoboinik, J. A.; Shaikhutdinov, S.; Freund, H. J. Support Effects on the Atomic Structure of Ultrathin Silica Films on Metals. *Appl. Phys. Lett.* **2012**, *100*, 151608.
(37) Wang, M.; Zhong, J.-Q.; Kestell, J.; Waluyo, I.; Stacchiola, D. J.; Boscoboinik, J. A.; Lu, D. Energy Level Shifts at the Silica/Ru(0001) Heterojunction Driven by Surface and Interface Dipoles. *Top. Catal.* **2016**, 1−11.
(38) Perdew, J. P.; Burke, K.; Ernzerhof, M. Generalized Gradient Approximation Made Simple. *Phys. Rev. Lett.* **1996**, *77*, 3865−3868.
(39) Giannozzi, P.; Baroni, S.; Bonini, N.; Calandra, M.; Car, R.; Cavazzoni, C.; Ceresoli, D.; Chiarotti, G. L.; Cococcioni, M.; Dabo, I.; et al. QUANTUM ESPRESSO: A Modular and Open-source Software Project for Quantum Simulations of Materials. *J. Phys.: Condens. Matter* **2009**, *21*, 395502.
(40) Vanderbilt, D. Soft Self-consistent Pseudopotentials in a Generalized Eigenvalue Formalism. *Phys. Rev. B: Condens. Matter Mater. Phys.* **1990**, *41*, 7892−7895.
(41) Blum, V.; Gehrke, R.; Hanke, F.; Havu, P.; Havu, V.; Ren, X.; Reuter, K.; Scheffler, M. Ab Initio Molecular Simulations with Numeric Atom-centered Orbitals. *Comput. Phys. Commun.* **2009**, *180*, 2175−2196.
(42) Deringer, V. L.; Lumeij, M.; Stoffel, R. P.; Dronskowski, R. Ab Initio Study of the High-Temperature Phase Transition in Crystalline GeO_2. *J. Comput. Chem.* **2013**, *34*, 2320−2326.
(43) Tucker, M. G.; Squires, M. P.; Dove, M. T.; Keen, D. A. Dynamic Structural Disorder in Cristobalite: Neutron Total Scattering Measurement and Reverse Monte Carlo Modelling. *J. Phys.: Condens. Matter* **2001**, *13*, 403.
(44) Villars, P. GeO_2 low-quartz (GeO_2 ht) Crystal Structure. http://materials.springer.com/isp/crystallographic/docs/sd_2080009 (accessed Apr 21, 2016).
(45) Kamakoti, P.; Barckholtz, T. A. Role of Germanium in the Formation of Double Four Rings in Zeolites. *J. Phys. Chem. C* **2007**, *111*, 3575−3583.
(46) O'Keeffe, M.; Yaghi, O. M. Germanate Zeolites: Contrasting the Behavior of Germanate and Silicate Structures Built from Cubic T_8O_{20} Units (T=Ge or Si). *Chem.—Eur. J.* **1999**, *5*, 2796−2801.
(47) Kasian, N.; Tuel, A.; Verheyen, E.; Kirschhock, C. E. A.; Taulelle, F.; Martens, J. A. NMR Evidence for Specific Germanium Siting in IM-12 Zeolite. *Chem. Mater.* **2014**, *26*, 5556−5565.
(48) Schlexer, P.; Giordano, L.; Pacchioni, G. Adsorption of Li, Na, K, and Mg Atoms on Amorphous and Crystalline Silica Bilayers on Ru(0001): A DFT study. *J. Phys. Chem. C* **2014**, *118*, 15884−15891.
(49) Loewenstein, W. The Distribution of Aluminum in the Tetrahedra of Silicates and Aluminates. *Am. Mineral.* **1954**, *39*, 92.
(50) Yakubovich, O. V.; Massa, W.; Gavrilenko, P. G.; Pekov, I. V. Crystal Structure of Chabazite K. *Crystallogr. Rep.* **2005**, *50*, 544−553.
(51) Lichtenstein, L.; Heyde, M.; Freund, H.-J. Atomic Arrangement in Two-Dimensional Silica: From Crystalline to Vitreous Structures. *J. Phys. Chem. C* **2012**, *116*, 20426−20432.
(52) Nash, A.; Nash, P. The Ni−Pd (Nickel-Palladium) System. *Bull. Alloy Phase Diagrams* **1984**, *5*, 446−450.
(53) Nash, A.; Nash, P. The Ni-Rh (Nickel-Rhodium) System. *Bull. Alloy Phase Diagrams* **1984**, *5*, 403−405.
(54) Bader, S. D.; Richter, L.; Orent, T. W. Auger-UPS study of intrinsic and Si-stabilized oxides of palladium. *Surf. Sci.* **1982**, *115*, 501.

DOI: 10.1021/acs.jpcc.6b07008
J. Phys. Chem. C 2016, 120, 26770−26781

(55) Orent, T. W.; Bader, S. D. LEED and ELS Study of the Initial Oxidation of Pd(100). *Surf. Sci.* **1982**, *115*, 323−334.
(56) Winkler, A.; Guo, X.; Siddiqui, H. R.; Hagans, P. L.; Yates, J. T. Kinetics and Energetics of Oxygen Adsorption on Pt(111) and Pt(112)- A Comparison of Flat and Stepped Surfaces. *Surf. Sci.* **1988**, *201*, 419−443.
(57) Dawson, C. J.; Sanchez-Smith, R.; Rez, P.; O'Keeffe, M.; Treacy, M. M. J. Ab Initio Calculations of the Energy Dependence of Si−O−Si Angles in Silica and Ge−O−Ge Angles in Germania Crystalline Systems. *Chem. Mater.* **2014**, *26*, 1523−1527.
(58) Dronskowski, R. *Computational Chemistry of Solid State Materials: A Guide for Materials Scientists, Chemists, Physicists and Others*; Wiley-VCH Verlag GMBH & Co.: Weinheim, Germany, 2005.
(59) Shannon, R. Revised Effective Ionic Radii and Systematic Studies of Interatomic Distances in Halides and Chalcogenides. *Acta Crystallogr., Sect. A: Cryst. Phys., Diffr., Theor. Gen. Crystallogr.* **1976**, *32*, 751−767.
(60) Fischer, F. D.; Sauer, J.; Yu, X.; Boscoboinik, J. A.; Shaikhutdinov, S.; Freund, H.-J. Ultrathin Ti-Silicate Film on a Ru(0001) Surface. *J. Phys. Chem. C* **2015**, *119*, 15443−15448.
(61) Maeda, T.; Kobayashi, Y.; Kishi, K. Growth of Ultra-thin Titanium Oxide on Cu(100), Fe/Cu(100) and Ordered Ultra-thin Iron Oxide Studied by Low-energy Electron Diffraction and X-ray Photoelectron Spectroscopy. *Surf. Sci.* **1999**, *436*, 249−68.
(62) Boffa, A. B.; Galloway, H. C.; Jacobs, P. W.; Benitez, J. J.; Batteas, J. D.; Salmeron, M.; Bell, A. T.; Somorjai, G. A. The Growth and Structure of Titanium Oxide Films on Pt(111) Investigated by LEED, XPS, ISS, and STM. *Surf. Sci.* **1995**, *326*, 80−92.
(63) Jennison, D. R.; Dulub, O.; Hebenstreit, W.; Diebold, U. Structure of an Ultrathin TiO_x Film, Formed by the Strong Metal Support Interaction (SMSI), on Pt nanocrystals on TiO_2(110). *Surf. Sci.* **2001**, *492*, 677−687.
(64) Boscoboinik, J. A.; Yu, X.; Shaikhutdinov, S.; Freund, H.-J. Preparation of an Ordered Ultra-thin Aluminosilicate Framework Composed of Hexagonal Prisms Forming a Percolated Network. *Microporous Mesoporous Mater.* **2014**, *189*, 91−96.
(65) dePaola, R. A.; Hrbek, J.; Hoffmann, F. M. Potassium Promoted C-O Bond Weakening on Ru(001). I. Through-metal Interaction at Low Potassium Precoverage. *J. Chem. Phys.* **1985**, *82*, 2484−98.

DOI: 10.1021/acs.jpcc.6b07008
J. Phys. Chem. C 2016, 120, 26770−26781